Determination of atomic form factors by means of coherent bremsstrahlung

M. Tobiyama
Department of Materials Science, Hiroshima University, Hiroshima 730, Japan

I. Endo, T. Monaka, Y. Sumi, H. Uchida, and N. Yamamoto
Department of Physics, Hiroshima University, Hiroshima 730, Japan

K. Yoshida and K. Watanabe
Institute for Nuclear Study, University of Tokyo, Tanashi 188, Japan

T. Ohba
School of Science and Engineering, Teikyo University, Toyosatodai, Utsunomiya 320, Japan

K. Baba
Hiroshima Shudo University, Hiroshima 731-73, Japan

T. Emura
Department of Applied Physics, Tokyo University of Agriculture and Technologies, Koganei 184, Japan
(Received 1 February 1991)

A method has been developed by means of coherent bremsstrahlung from a single crystal for the determination of atomic form factors. This method employs a precise measurement of energy spectra of γ rays in the several-hundred-MeV region produced by 1.2-GeV electrons from single crystals as a function of the relative angle between a definite crystal axis and the incident-electron beam. It is shown that the spectra contain the electron-screening effect around the target nuclei and give information on the atomic form factor mainly at small momentum transfers. Possible problems with this method have been examined with this experiment using a silicon crystal. A method to analyze the experimental results has been established and with this method the deviation of atomic form factor from theoretical calculation is detectable at a level of down to a few percent. The present experimental data for a silicon crystal are consistent with the form factor obtained by the *Pendellösung* method, which shows small deviations from the Hartree-Fock model at small momentum transfers. The accuracy attained in this method has been shown not to be too much affected by the imperfections of the crystal, at least for dislocation densities of up to 10^4 cm^{-2}.

I. INTRODUCTION

The atomic form factor is one of the most fundamental physical quantities in solid-state physics. It is the Fourier transform of an electron distribution around a nucleus and carries information on the electron wave function. Precise knowledge of the atomic form factor also has practical significance, as may be exemplified by the problem associated with the computation of x-ray attenuation coefficients.[1] It is in general impossible to calculate the atomic form factor exactly, because it needs an exact solution for a complicated many-body problem. There are some calculations[2,3] using approximate methods which are believed to be accurate enough in practical use for some materials. The adequacy of these theoretical treatments, however, should be verified experimentally. Furthermore, it should be noted that the atomic form factor in aggregate may be slightly different from that of an isolated atom. The quality of existing data is inadequate for answering these problems and more detailed measurements are desirable.

Most measurements to determine the atomic form factor performed up to now are mainly by means of x rays[4] or low-energy electrons.[5] The x-ray experiments may be classified into two groups; kinematical and dynamical methods. In the former method, integrated intensities of diffraction images from a single crystal or powder are measured. This method has been applied to many kinds of materials. The most serious problem in the method is that absolute measurement is not possible and that absorption or extinction corrections are necessary. On the other hand, the absolute value of the form factor is obtainable by use of the dynamical method. Nevertheless, as the method needs a crystal which is perfect with relatively large physical dimensions, there are few kinds of crystal which are appropriate for use with the method. It is therefore highly desirable to develop a method which is not sensitive to the imperfections in the target crystal.

The photon spectra of coherent bremsstrahlung from high-energy electrons have been found to be very sensitive to the atomic form factor of the target material.[6,7] This means that a precise measurement of such photon

spectra may give us new information on atomic form factors. In addition, the information obtained in this way is complementary to that obtained from x-ray measurements in a sense that the former information reflects the electron screening around nuclei, while the latter directly reflects the electron distribution around nuclei.

In the coherent bremsstrahlung experiment stated above, all the real particles such as the incident and recoil electron and the emitted photon have their momentum of the order of several hundred MeV or higher. As the corresponding wavelength is far smaller than the size of atomic structure and rather closer to the nuclear size, they may be regarded to interact only with the nuclear field. The momentum transfer from incident electron to nucleus, on the other hand, ranges from keV to several hundred MeV. The phonon associated with the atomic vibration can interact with slow electrons surrounding nucleus but not with such high-energy electrons as in the present case. As a result, the phenomenon of our interest is free from any complexity inherent to dynamical treatment of keV electrons[8] and the plane-wave approximation is well valid.

Possible problems in the method using coherent bremsstrahlung are as follows.

(i) It is generally difficult to measure the energy spectra of high-energy γ rays precisely enough to discuss the small deviation of the spectral shape.

(ii) The method requires considerably complicated experimental technique and long time consumption. Moreover, there may be no guarantee of the reproducibility for the experimental system in some cases.

(iii) By a radiation damage, the target crystal may be broken to some extent.

(iv) The dislocation of the target crystal may heavily affect the result obtained in the method.

We have already tested the feasibility of the coherent bremsstrahlung method and reported that we could reproduce the shape of the photon spectra for the perfect silicon crystal.[9] As most precise experiments were made for silicon by measuring *Pendellösung* fringes using wedge-shaped crystal,[10–12] a silicon crystal may be the most suitable for checking a method to determine the atomic form factor.

We have performed the present experiment to clarify the possible problems stated above. We have constructed a detector with improved control system. In order to check the reliability of this kind of measurements, we have prepared two kinds of silicon crystal; one is a perfect crystal which is the same one as in the previous experiment and the other is a crystal in which a heavy dislocation has been intentionally introduced.

Firstly, we briefly describe a theoretical background for coherent bremsstrahlung in Sec. II. Secondly, in Sec. III, we give an explanation of the present experimental set-up. Section IV is devoted to a description of our experimental procedure, data analysis, and experimental results. In Sec. V, the present results are compared with the results of x-ray experiments and also given are the discussions on the validity of the present method and on other related problems. Finally our conclusion is summarized in Sec. VI.

II. COHERENT BREMSSTRAHLUNG

A. Theoretical foundation

A bremsstrahlung process is diagrammatically represented in Fig. 1, where an electron with energy E_0 and momentum $\mathbf{p}_0$ is deflected by the potential shown by a blob and emits a photon with momentum $\mathbf{k}$. Let the energy and momentum of the final-state electron be denoted by E and $\mathbf{p}$, respectively, the energy and momentum conservation law read

$$\mathbf{p}_0=\mathbf{p}+\mathbf{k}+\mathbf{q} , \tag{1}$$

$$E_0=E+k , \tag{2}$$

where $\mathbf{q}$ is the recoil momentum of the nucleus. The recoil energy corresponding to $\mathbf{q}$ can be neglected because of the large mass of the recoiling nucleus. Here, and henceforth, we use the natural unit in which $m_e=c=\hbar=1$, where m_e is the electron mass. Conversion of the momentum transfer $\mathbf{q}$ in this natural unit to the $[\lambda(\text{Å})^{-1}\sin(\theta/2)]$ unit is accomplished by multiplying a factor 20.607 44, which is convenient to represent the momentum transfer in the Rayleigh scattering for the wavelength λ and the deflection angle θ.

At very high energies where the bremsstrahlung is strongly collimated in the forward direction, $\theta_k \lesssim 1/E_0$, the longitudinal and transverse momentum transfer q_l and q_t, respectively, with respect to the incident-electron direction are restricted by the relations

$$\delta \le q_l \lesssim 2\delta , \tag{3}$$

$$0 \le q_t \le 2x , \tag{4}$$

where δ is the minimum recoil momentum given by

$$\delta=\frac{x}{2E_0(1-x)} , \tag{5}$$

with $x=k/E_0$ the relative photon energy. Outside the region defined above, the bremsstrahlung is either inhibited or negligibly small.

Though δ grows rapidly when x approaches unity, it is usually a very small quantity compared to the other momenta involved. Thus, the kinematically allowed region for momentum transfer forms a very thin disc of which the thickness is about δ and the radius is of the order of

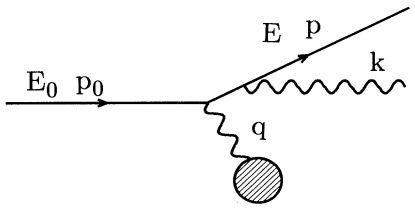

FIG. 1. Momentum and angular relations in electron bremsstrahlung. The incident-electron momentum, scattered electron momentum, photon momentum, and momentum transfer are denoted by $\mathbf{p}_0$, $\mathbf{p}$, $\mathbf{k}$ and $\mathbf{q}$, respectively.

unity. It is axially symmetric with respect to the initial electron momentum $\mathbf{p}_0$ and it stands at the distance δ from the origin of the interaction as visualized in Fig. 2.

Using the first-order Born approximation, we obtain the Bethe-Heitler expression[13] for the differential cross section for an isolated atom. According to the Bethe-Heitler formalism, the atomic electrons surrounding the nucleus make partial screening of the nuclear charge. This screening effect is represented in terms of the atomic form factor $F(q^2)$, which is the Fourier transform of the charge distribution $\rho(r)$ around the nucleus;

$$F(q^2)=\int e^{i\mathbf{q}\cdot\mathbf{r}}\rho(r)d^3r \ . \tag{6}$$

For an ideal crystal at zero temperature, the momentum transfer is not permitted except at the reciprocal lattice points due to the periodic nature of the potential. From the conditions (3) and (4), only the reciprocal-lattice points which enter the thin disc region can contribute to the bremsstrahlung process in this case.

At finite temperature, however, we must take into account the effect of thermal oscillation, and the differential cross section is expressed by the sum of the coherent contributions and the incoherent ones;[14]

$$\frac{k}{\sigma_0}\frac{d\sigma}{dk}=[1+(1-x)^2](\psi_1^i+\psi_1^c)-\tfrac{2}{3}(1-x)(\psi_2^i+\psi_2^c) \ , \tag{7}$$

where

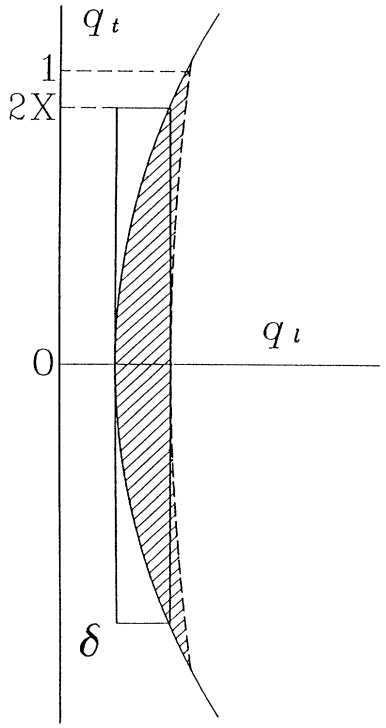

FIG. 2. The thin disc region (shaded area). Its thickness δ is far smaller than x or q. The upper kinematical boundary for $\mathbf{q}$ is drawn only schematically.

$$\sigma_0=\frac{Z^2}{137}\left[\frac{e^2}{m_ec^2}\right]^2=0.5794\times10^{-27}Z^2 \text{ cm}^2 \ ,$$

$$\psi_1^i=4+4\int_\delta^1(1-e^{-Aq^2})\frac{[1-F(q^2)]^2}{q^4}(q-\delta)^2q\,dq \ ,$$

$$\psi_2^i=\frac{10}{3}+4\int_\delta^1(1-e^{-Aq^2})\frac{[1-F(q^2)]^2}{q^4}\times\left[q^2-6\delta^2\ln\left[\frac{q}{\delta}\right]+3\delta^2-4\frac{\delta^3}{q}\right]q\,dq \ ,$$

$$\psi_1^c=\frac{1}{2}\frac{(2\pi)^2}{a^3}\sum_{\mathbf{q}=\mathbf{g}}|S(\mathbf{q})|^2e^{-Aq^2}\frac{[1-F(q^2)]^2}{q^4}\frac{\delta q_t^2}{q_l^2} \ ,$$

$$\psi_2^c=3\frac{(2\pi)^2}{a^3}\sum_{\mathbf{q}=\mathbf{g}}|S(\mathbf{q})|^2e^{-Aq^2}\times\frac{[1-F(q^2)]^2}{q^4}\frac{\delta^2q_t^2(q_l-\delta)}{q_l^4} \ ,$$

with a being the lattice constant. The superscripts i and c denote the incoherent part and coherent part, respectively. We used A for the thermal oscillation constant

$$A=\frac{3m_e^2c^2}{4Mk_B\Theta_D}\left[1+4\left[\frac{T}{\Theta_D}\right]\Gamma\left[\frac{\Theta_D}{T}\right]\right] \ , \tag{8}$$

where M is the atomic mass of the crystal, k_B is the Boltzmann constant, Θ_D and T are the Debye temperature and the absolute temperature of the crystal, respectively. We also introduced the structure factor $S(\mathbf{q})$. The summation in the coherent part should be done over the reciprocal lattice points $\mathbf{g}$ kinematically allowed, i.e., mainly those in the thin disc region.

B. Dip-bump structures

We show in the following the qualitative behavior of the differential cross section. For most conditions, the incoherent part depends weakly on x and is a slowly varying function of k. On the other hand, the coherent part depends strongly on both x and the direction of the crystal.

We first investigate the case where the incident electron enters parallel to one of the crystal axes, [110]*. For the lower boundary of the thin disc to reach the first row of reciprocal lattice points, δ is equal to $\sqrt{2}\times2\pi/a=9.6\times10^{-3}$ in the case of a silicon crystal. Choosing $E_0=1.2$ GeV$=2.3\times10^3$ in the present unit, we find that the corresponding x is 0.98. This is very close to the end of the spectrum, where the momentum transfer is so large that the intensity of coherent contribution is very small with respect to the incoherent one. The cross section has therefore no appreciable enhancement in the coherent part.

Next, we consider the case where the incident electron enters the crystal with a small angle θ with respect to the

axis [110]* as seen in Fig. 3(a). Now, for a certain photon energy k_0, the thin disc intersects the (110) plane, as shown in Fig. 3(b). This gives a large enhancement in the cross section. While rotating the crystal in the $(1\bar{1}0)$ plane to decrease θ, it happens that the lower boundary of the thin disc moves away from the first row. Then, the contributions from the first row suddenly disappear and the cross section drops accordingly. With decreasing θ further, the cross section again increases and reaches the maximum when the lower boundary is just on the third row. Thereafter the cross section decreases with decreasing angle, thus, resulting in a dip-bump structure in angular dependence.

A similar argument is applicable to the case where we vary the photon energy for a fixed incident angle; we first assume that the thin disc intersects the (110) plane as shown in Fig. 3(a). With increasing photon energy from k_0, the lower boundary of the thin disc proceeds away from the origin. The cross section grows with the photon energy and has the maximum when the lower boundary of the thin disc reaches the first row. The cross section suddenly drops when the lower boundary crosses the row.

The above mechanism gives a specific dip-bump structure in the coherent bremsstrahlung spectrum which is to be observed in the present experiment.

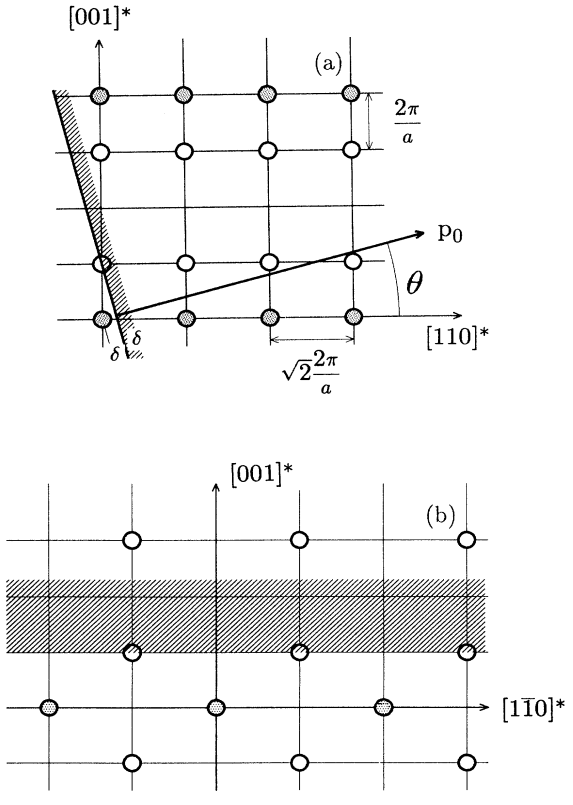

FIG. 3 (a) The direction of the incident-electron momentum $\mathbf{p}_0$ is directed through a small angle θ in the plane $(1\bar{1}0)$. (b) The thin disc now includes the reciprocal-lattice points in the (110) plane.

C. Effect of the atomic form factor

In ordinary x-ray experiments, the intensity of the diffraction image is proportional to $|F(q^2)|^2$, while the coherent part of the bremsstrahlung spectrum is proportional to the factor $[1-F(q^2)]^2/q^4$.

The discussion of the previous section shows that the specific dip-bump structure of the coherent bremsstrahlung comes from the lattice structure of the crystalline target and that the intensity of the spectrum is inversely proportional to the fourth power of the momentum transfer which corresponds to the distance in the reciprocal-lattice space. Now, it is clear that a possible small deviation in the atomic form factor at small momentum transfer may result in a large deviation in the coherent bremsstrahlung intensity.

III. EXPERIMENTAL SET-UP

A. General consideration

We have a few methods to determine the energy of photons emitted in the bremsstrahlung process. The first one is to measure the momenta of e^+-e^- pair which is converted from a photon, which is known as pair spectrometry. In this method, though a good energy resolution can be achieved, the time needed to get the photon spectrum is huge. Another direct-measurement method is to convert the photon to an electromagnetic cascade shower. To get a good accuracy, we must keep the intensity of the photon beam low so that only one photon will enter the detector in one trigger signal. The data amount to a large magnitude and the time needed to get one photon spectrum is accordingly long.

Instead of these direct measurements, we adopt the following indirect method: if we know both the energy of the incident electron, E_0, and that of the final electron, E, we can determine the photon energy k by the relation $k=E_0-E$. We place an analyzer magnet downstream from the target. The electron which emits a photon has a smaller curvature in the magnetic field compared with the electrons which do not emit any photon and therefore appears at different exit point of the analyzer magnet. We place a counter hodoscope downstream from the analyzer magnet and measure the momentum of a recoil electron by its hit position on the hodoscope. This method is called the tagging method because the energy of all the photons is tagged by the momentum of the recoil electron. As we do not need to identify the individual photons, we only count the number of the recoil electrons which hit any of counter elements of the hodoscope. The counting rate in this case can be increased until it reaches limiting counting rate for single electrons.

As the characteristic feature of the coherent bremsstrahlung appears in the lower photon energy region, we mainly confine ourselves to employ a hodoscope which can measure high-energy recoil electrons.

Since we had to remove the error due to the differences in the energy acceptances for different counter elements of the hodoscopes, we took the ratio of each spectrum to the standard one which was obtained for the polycrystal-

line aluminum target under the standard conditions. Hereafter, this ratio is referred to as the normalized spectrum.

As it is difficult to extract beam with high enough stability and to make a direct measurement of beam intensity upstream from the target without disturbing the beam properties, we count the number of electrons of 1.2 GeV by a thick-walled ionization chamber placed downstream from the analyzer magnet.

To vary the direction of the crystalline target relative to the incident-electron beam, we use a high-precision goniometer which is controlled by a personal computer at the counting room.

B. Electron synchrotron

The electron synchrotron and the tagging system at the Institute for Nuclear Study, University of Tokyo, was used[15] in this experiment. The circulating electrons lose their energy in an absorber and are kicked out to the external beam line by two fast kickers. The beam line is schematically shown in Fig. 4. It has two lead slits that can collimate the electron beam in both vertical and horizontal directions.

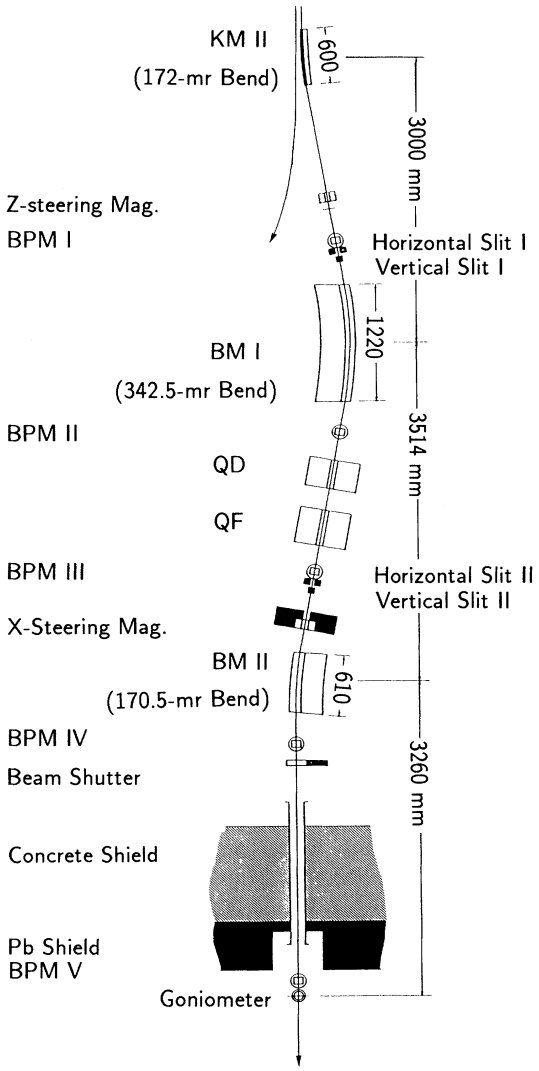

FIG. 4. The layout of the electron extraction beam line. BM: bending magnet. KM: pulsed kicker magnet. BPM: beam profile monitor.

At the first collimator, the beam is scraped to ± 1 mm in both vertical and horizontal directions. The secondary electrons which are created at the first collimator are scraped out by the second collimator. The quadrupole magnets are tuned to make the beam divergence at the target position as small as possible.

C. Tagging system and electron monitor

The tagging system consists of the analyzer magnet and two counter hodoscopes as shown in Fig. 5. The magnet supplies a magnetic field of 1.17 T and an effective field length of 0.8 m. The high-energy electrons from the accelerator, after hitting a target material, enter this magnetic field and give their trajectories according to their momenta.

There are two kinds of counter hodoscopes of plastic scintillators. One is for low-energy electrons, the other is for high-energy ones. The spread of the electron beam due to the multiple scattering in the target material is not

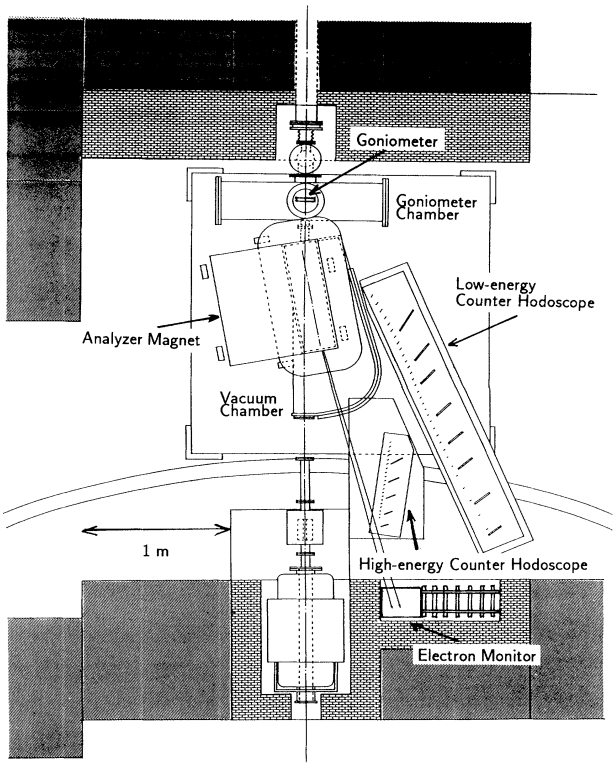

FIG. 5. The layout of the tagging system. The electron beam comes from the upper side of the figure and enters the crystalline target on the goniometer. Electrons are analyzed according to their momenta by an analyzer magnet. There are two sets of counter hodoscope. Downstream from the analyzer magnet, there is a thick-walled ionization chamber which counts the number of extracted electrons.

negligible because the analyzer magnet is horizontally defocusing. In the case of 0.5-mm silicon target, the spread of the beam at the hodoscope is calculated to have a width corresponding to the energy spread of 20 MeV. We designed the energy acceptance of each bin to be 20 MeV. The corresponding horizontal size of the scintillators ranged from 10.6 to 19.0 mm.

An energy calibration using an electron beam has shown that the hodoscope covers the energy range from 975 to 600 MeV with bin width ranging from 15 to 20 MeV. The nonuniformity in the acceptance is irrelevant to our experimental results because we are concerned only with the ratio of coherent spectrum to incoherent one.

The low-energy hodoscope has a resolution of 10 MeV, covering an energy range between 100 and 370 MeV. We use this hodoscope for calibration and monitoring of the electron beam.

The thick-walled ionization chamber is made of one 2-cm-thick copper wall, and twenty-three 1-mm-thick copper plates. The extracted beam intensity was about $2\times10^8\ e^-/s$.

D. Target and goniometer

Two kinds of high-purity silicon single crystal were used to observe the effect of crystal imperfection. One is a dislocation-free, perfect crystal and the other is a crystal which has dislocation with a density of $\sim10^4\ cm^{-2}$. They have been provided by Shin-etsu Handoutai Co. Ltd. It is hard to introduce dislocations heavier than in the present case into a silicon crystal without making cracks.

The crystals used in the experiment were wafers with a thickness of 0.5 mm and dimensions of 20 mm×20 mm. The surface of the target crystal is (110) and the edges are parallel to $[\bar{1}11]$ and $[1\bar{1}2]$ within an accuracy of 0.5° The orientation of the target crystal was determined by the back reflection Laue method.

The goniometer has three axes which cross at one point and one translational moving axis as shown in Fig. 6. Around each axis, rotation is made by a stepping motor in vacua and the position is informed through rotary encoders. The possible range of rotation is $-30.000°\sim210.000°$ for the ψ axis, $-30.000°\sim30.000°$ for the ϕ axis and $0.000°\sim180.000°$ for the θ axis with a common precision of 0.005°. The crystalline target is mounted on a holder which has a circular opening window of 20 mm in diameter for the beam. The crystal must therefore be larger than 20 mm at least in one direction to be mounted on the holder.

Sliding the goniometer transversal to a beam line, we can use a polycrystalline material as the target. The polycrystalline radiators used are a 0.5-mm-thick aluminum strip, an aluminum wire of 0.5 mm in diameter and a 50-μm platinum strip. The frame of these targets is far from the beam and has no appreciable contribution to the spectrum.

E. Data acquisition methods

We counted the number of electrons by using the full range of the high-energy hodoscope, eight elements of the low-energy hodoscope and the electron monitor. We used a special TAG module which can convert the signal from photomultipliers to NIM level signals through the discriminators and the coincidences. The CAMAC 24-bit scalars are used. The CAMAC system and the goniometer are controlled by a personal computer PC-9801RA4 with use of the on-line code programmed with Turbo PASCAL Version 4. The goniometer and the scaler were computer controlled. The temperature of the crys-

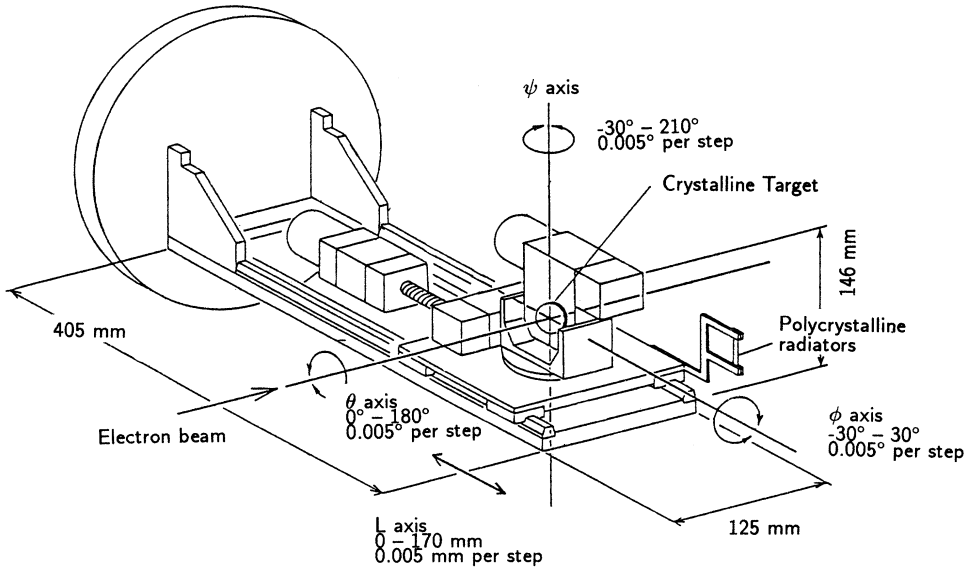

FIG. 6. Whole view of the goniometer. It has three axes which cross at one point with each other. It is placed in a vacuum chamber.

tal holder of the goniometer was monitored by three thermistors.

IV. EXPERIMENTAL PROCEDURE

A. Check runs

The number of data sets obtained in this experiment is summarized in Table I. To estimate the contribution of the secondary electrons produced in the beam line to the main spectrum, we measured the energy spectrum of electrons with the target removed. Two types of *empty runs* were carried out occasionally. The first type is *completely empty* runs whose data are taken at the transverse position of the goniometer completely far away from the beam line. The obtained ratio of the spectrum for the *completely empty* to that for Al target ranged from 0.6% to 1% for the high-energy hodoscope and 1.5% to 4% for the low-energy hodoscope.

The other is *empty-holder* run for which we set the goniometer at the normal position but without target crystal. Because the opening window of the holder is not large enough to avoid the contribution from the beam halo, the obtained empty ratio is larger than that in the *completely empty* case. The ratio in this case to the Al spectrum amounted to 3–4.5 % and 9–11 % for high- and low-energy hodoscopes, respectively. We performed *completely empty* runs and *empty-holder* runs seven times each.

We used the incoherent bremsstrahlung spectra for a calibration of the energy acceptance of the tagging channels and for the checking of the reliability of the system. The polycrystalline target of 0.5-mm aluminum strip with a thickness of 0.5 mm was used for this purpose. Since the beam condition might change in time, the incoherent bremsstrahlung runs were performed from time to time, seven times in total. The spectra of two adjacent incoherent runs were found to be the same within a deviation less than 0.1%. The incoherent bremsstrahlung spectra from an aluminum strip measured in 10 s is shown in Fig. 7.

TABLE I. The number of all data obtained in this experiment.

Run name	ψ axis		Number of data
Completely empty			15
Empty holder			200
Normalization run			20
Perfect Si crystal		Check run	910
	[001]*	search	850
	[001]*	high statistics	330
	[$\bar{1}$10]*	search	720
	[$\bar{1}$10]*	high statistics	70
Imperfect Si crystal		Check run	340
	[001]*	search	270
	[001]*	high statistics	60
	[$\bar{1}$10]*	search	770
	[$\bar{1}$10]*	high statistics	90

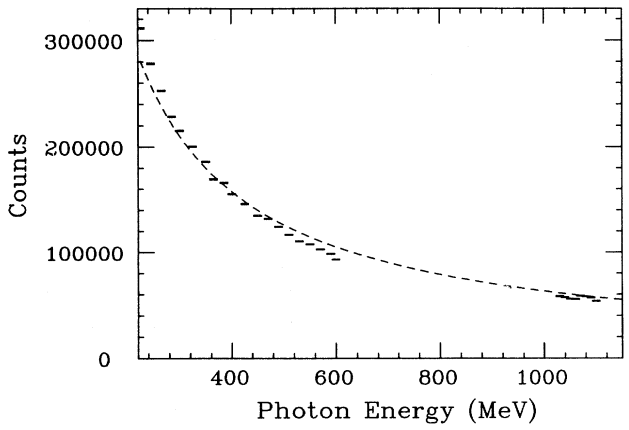

FIG. 7. The incoherent bremsstrahlung spectrum measured in 10 s from the Al polycrystalline radiator. The errors are due to statistics only. The dashed curve is the fitted $1/k$ curve.

B. Silicon runs

We mounted the crystalline target on the holder in such a way that the (110) plane of the crystal faced the incident beam with one edge of [$\bar{1}$11] directed to the vertical when both of the goniometer angles ϕ and θ were 0°. By rotating the target around the θ axis, the symmetry axis was made to be parallel to the ψ axis. The symmetry axes we have chosen were [2$\bar{2}\bar{1}$]*, [$\bar{1}$10]*, and [001]*.

First, rotating one axis while leaving the others unchanged, we observed the orientational dependence of the spectrum and searched for the symmetry center. Next, fixing this temporary symmetry center, we rotated the target around the other axis and searched for another symmetry center. We repeated this process until we confirmed the two symmetry axes. For example, in order to align a [$\bar{1}$10]* axis vertically, it took five survey runs to establish the required symmetry. Each set of runs includes about 80 sets of data. At the angular position where the coherent enhancement at the low photon-energy counter reaches its maximum, the counting rate increases to 80 k counts/s. To take one data set at any angular position, it took about 10 s.

After having established the relation between the angle of the goniometer and the direction of the crystal target relative to the extracted electron beam, we rotated one axis and made a precise measurement of the spectrum, which needed about 2 min to get one set of data.

The spectrum from the imperfect silicon crystal is obtained in a manner completely similar to the perfect-silicon-crystal case.

C. Data reduction and results

Since the crystal holder of crystalline target partially intercepts the beam halo, we correct the data for the crystalline target by using the *empty-holder* data. In the case of the data for polycrystalline target, the contribution from the target holder is negligible. We compensated the data for the polycrystalline target using the results

of *completely empty* runs.

We show the orientational dependence of the normalized spectrum on several selected counters of the hodoscopes in Fig. 8(a) for the perfect silicon crystal where the ϕ axis is set at the symmetry center, $\phi=-1.756°$. The abscissa is the angle ψ of horizontal rotation, while the ordinate is the ratio of counts I(crystalline silicon)/I(polycrystalline aluminum) normalized to the same count of the electron monitor. The error bars are due to statistical effects only. We clearly see the symmetric behavior with respect to the crystal axis [110]* and this behavior has a good reproducibility. The farthest peaks from the symmetry center correspond to the enhancements when the thin disc region intercepts the reciprocal lattice points on the line defined by $\bar{1}11$ and $1\bar{1}1$. The second and the highest peaks correspond to the line of $\bar{1}13$ and $1\bar{1}3$, and so on. The peaks move with photon energy, being consistent with the theoretical prediction in Sec. II.

Figure 8(b) shows the orientational dependence of the normalized spectrum for the imperfect silicon crystal where the ϕ axis set at the symmetry center $\phi=-0.978°$. Almost the same structure as in the case of perfect silicon crystal can be seen.

Very close to the symmetry center, $\psi_c=2.299°$ for the perfect silicon crystal in Fig. 8(a), 0.5° for the imperfect one in Fig. 8(b), the curve of the normalized spectrum has a small peak which is not predicted by theory as reported earlier.[16] In such a region, however, the approximation used in the theory of coherent bremsstrahlung is not valid.

To see the effect of the atomic form factor to the spectrum, let us examine the normalized spectrum when the thin disc is near the line of $\bar{1}11$ and $1\bar{1}1$ mentioned above. Figure 9 shows the normalized spectrum of the perfect silicon crystal where $\psi=2.299°$. The solid curve shows the calculated spectrum for the Hartree-Fock form factor[2] and there is a good agreement between the experimental and the theoretical curves besides a slight difference near the peak of the normalized spectrum, where the theoretical curve lies below the experimental data. This behavior is kept unchanged during the experiment and hence not due to the radiation damage effect.

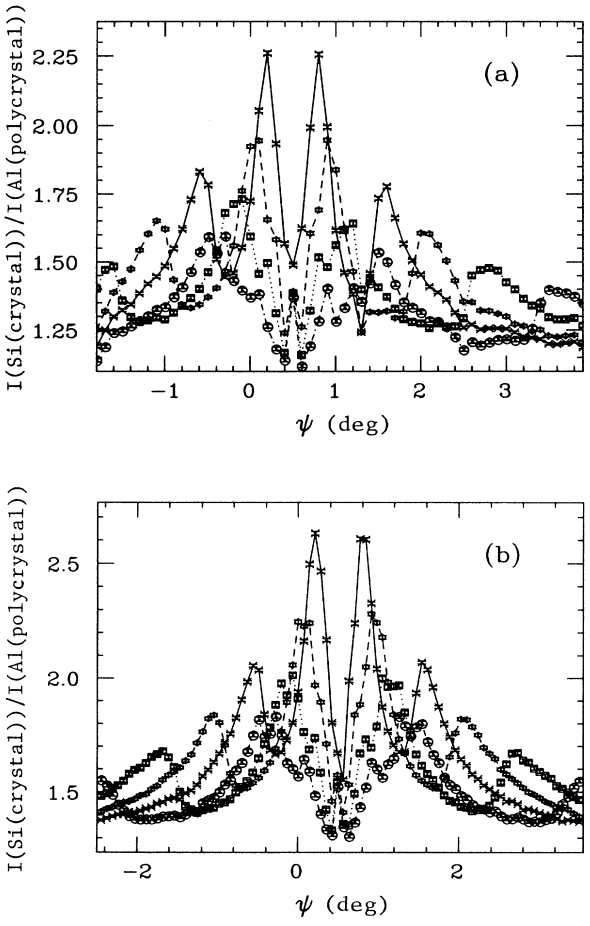

FIG. 8. The orientational dependence of the normalized spectra of (a) perfect Si crystal and (b) imperfect Si crystal. The abscissa is the horizontal rotation ψ. The symmetry axis is [$\bar{1}10$]. The photon energies are 300 (solid curve), 300 (dashed), 510 (dotted) and 600 MeV (dot dashed). The error bars are due to statistics only.

V. DISCUSSION

A. Theoretical calculation

We compare the present experimental results with the theoretical calculations which employ Eq. (7) and various types of form factors. Since the differential cross section for the coherent spectrum is quite sensitive to the direction of the crystal axis, we need to know the degree of the goniometer misalignment and of the beam divergence for more precise discussion. The misalignment of the goniometer is determined from the measured differences between two positions of symmetry axes where $|\Delta\theta|$ is about 90°. The electrons undergo the multiple elastic scattering in the target. As the scattering does not de-

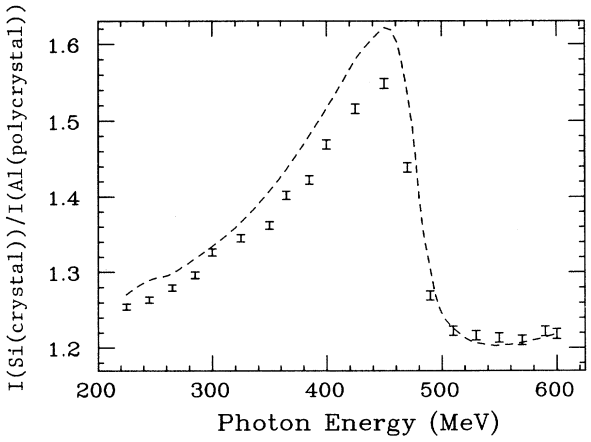

FIG. 9. Normalized spectrum of perfect Si crystal where the thin disc is near the [$\bar{1}11$] line, $\psi=2.299°$, $\Delta\psi=\psi-\psi_{\text{center}}$ is 1.8°. A theoretical calculation based on the Hartree-Fock model are also shown by the dashed curve.

pend on the periodicity of the crystal, we adopt the ordinary formula for average angular deviation θ_0 for amorphous materials:

$$\theta_0=\frac{14.1\ \text{MeV}/c}{p\beta}\sqrt{L/L_R}\left[1+\tfrac{1}{9}\log_{10}(L/L_R)\right], \quad (9)$$

where p and β are the momentum (in MeV/c) and velocity of the incident particle, respectively, and L/L_R is the thickness, in units of radiation length of the scatterer. Since the scattering effect has azimuthal symmetry, we get the same multiple scattering divergence $\delta\theta_m=0.0368°$ in both horizontal and vertical directions. With the beam divergence of $\delta\theta_b=0.009°$ in both direction, we finally get the total directional divergence of the beam using the following relation:

$$(\delta\theta)^2=(\delta\theta_b)^2+(\delta\theta_m)^2 ,$$

which leads to $\delta\theta=0.0379°$ for both ψ and ϕ directions. In the calculation, we summed spectra from the 10 angular values for both vertical and horizontal directions with the Gaussian-type weight whose standard deviation is given by $\delta\theta$.

In order to take into account the effect of the energy acceptances of the counter hodoscope, we calculate the differential cross section for the three photon energies $\Delta E=E-E_{\text{set}}=-7$, 0, and $+7$ MeV for each energy bin, and then took the mean of the results for these three points.

We make an ellipsoid of revolution that contains normal thin disc region completely to choose the reciprocal lattice points which contribute to the spectrum in the calculation. It is insufficient to count the reciprocal lattice points only in the normal thin disc region to attain an accuracy high enough to distinguish the difference between the form factors because the longitudinal momentum transfer has no upper limit. We added a few more points out of the ellipsoid and checked the magnitude of their contribution. The upper-limit point we adopted has a contribution of at most 5×10^{-5} of that of the boundary points in the ellipsoid.

The measured temperature near the crystal holder was from 30 °C to 40 °C due to the heat transfer from the stepping motors of the goniometer. As the Debye temperature of silicon is high enough, the variation of the temperature contributes very little in the present case. We have chosen a temperature of 40 °C in the calculation.

The incoherent bremsstrahlung spectrum for the aluminum target is given in a published table.[4] We finally obtain the result in a form of (spectrum from the crystalline target)/(spectrum from the polycrystalline target).

B. Comparison with other x-ray experiments

The experimental results for the perfect silicon crystal are compared with the calculations which employ the Hartree-Fock (HF) form factor.[2] In order to simplify our calculation, we expand the form factor in the following form by means of the least-squares method:

$$F(q^2)=\sum_{i=1}^{7} a_i\exp(-b_i q^2)+c . \quad (10)$$

The fitted coefficients are shown in Table II.

The calculated normalized spectrum is given in Fig. 9 by the dashed curve, which is to be compared with the experimental data for the angular divergence being $\Delta\psi=1.8°$ and $\Delta\phi=0°$ with respect to the symmetry axis. The experimental data lie somewhat lower than the HF curve near the peak of the spectrum. It is, however, difficult to regard the difference observed between experimental data and the calculation as due to the inadequacy of the form factor used because the theoretical treatments we have adopted have uncertainties of the order $\alpha=1/137$, the fine-structure constant, whereas the observed difference is also of this order. It may be a systematic error in the theoretical calculation. On the other hand, if we assume that the difference is due to the deviation in the atomic form factor, the resulting form factor should be slightly increased in comparison with the HF form factor.

The form factor of Si crystal is known to an accuracy of 0.05% from the measurement with the *Pendellösung* method by Saka and Kato.[10] They showed that the form factor of 111 reflection, the lowest reflection, has the largest deviation from the HF form factor. In our case, since the calculated curve is the sum of the contribution from many reciprocal lattice points, it is generally impossible to uniquely determine which part of $F(q^2)$ is to be modified. We first follow the result from Saka and Kato. We have tried to fit our results adding the following extra Gaussian term:

$$a\frac{1}{\sqrt{2\pi}\sigma}\exp\left[-\frac{1}{2}\frac{(x-\mu)^2}{\sigma^2}\right], \quad (11)$$

of which standard deviation is $\sigma=0.02$ Å^{-1}. We first fixed the center of the extra Gaussian to the 111 ($\mu=0.16$ Å^{-1}) and varied the height a to reproduce our experimental result. Figure 10(a) shows the result in the case of $a=0.02$ whose form factor differs from the HF form factor by about 3.3% at 111. The original HF form factor and the modified one are compared in Fig. 11 as functions of the momentum transfer. This modified form factor can reproduce the present experimental results very

TABLE II. The atomic form factor of Si expressed in the form of $F(q^2)=[\sum_{i=1}^{7} a_i\exp(-b_i q^2)+0.018\,712]/14$.

a_1	a_2	a_3	a_4	a_5	a_6	a_7
7.445 6	3.350 9	1.681 8	1.5049	1.3791×10^{-4}	1.5653×10^{-4}	1.3791×10^{-4}
b_1	b_2	b_3	b_4	b_5	b_6	b_7
1.9520	28.745	0.069 804	89.377	9114.2	51.779	9994.0

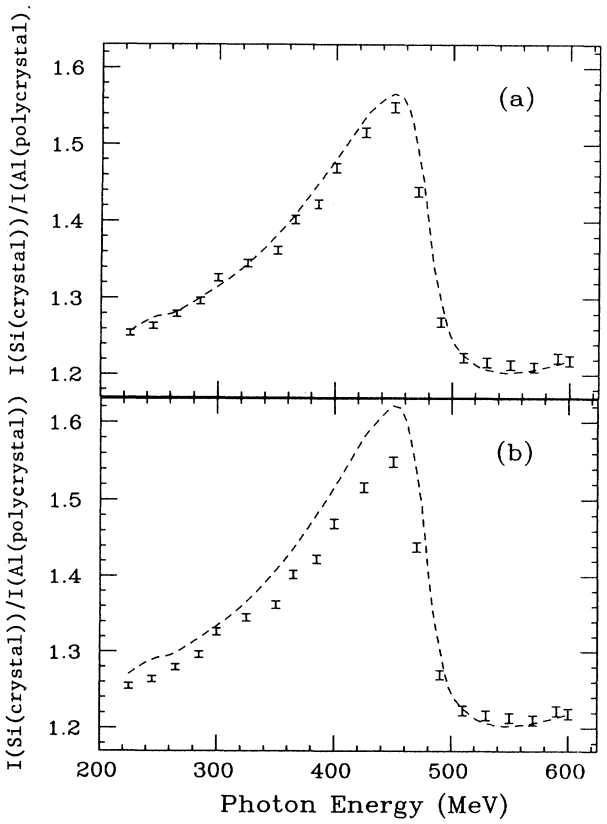

FIG. 10. Normalized spectrum with the calculated result of which form factor is modified by adding an extra Gaussian. (a) The extra Gaussian with $\mu=0.16$ Å^{-1}, $\sigma=0.02$ Å^{-1}, $a=0.02$ is added. (b) The extra Gaussian with $\mu=0.26$ Å^{-1}, $\sigma=0.02$ Å^{-1}, $a=0.02$ is added.

well.

If we change the center of the extra Gaussian to 220 point ($\mu=0.26$ Å^{-1}) keeping its height unchanged, the fit becomes worse as shown in Fig. 10(b), implying that the 111 reflection mainly contributes to the enhancement. Both of the present analyses and that by the *Pendellösung* method suggest the same trend of deviation from the HF form factor at 111, but the deviation in our case is larger than the latter; in our case, the deviation from the HF form factor is 3.3% whereas that for the latter is 1.9%. This difference may be regarded as a consequence of a systematic error in our theoretical calculation.

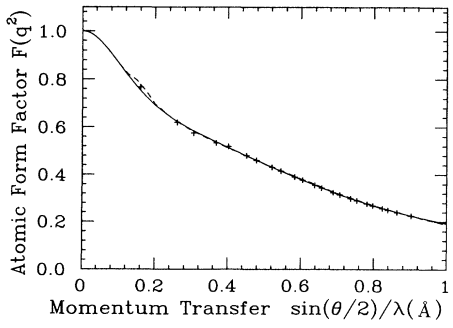

FIG. 11. The atomic form factor of the HF model (solid curve) and a modified one whose center of extra Gaussian is 0.16 Å^{-1} (111 reflection) (dashed). The marks are the results from the *Pendellösung* method.[10]

C. Effect of the imperfection of crystal

If the target silicon crystal has dislocations, the reciprocal-lattice points become fuzzy. This is equivalent to increase the beam divergence for the perfect silicon crystal. This effect will reduce the normalized spectrum to some extent.

The spectrum obtained from the imperfect silicon target is analyzed by employing the same method as that for the perfect one. The symmetry center was $\psi=0.55°$ and $\phi=-0.978°$, as shown in Fig. 8(b). The structure of the orientational dependence of the spectra is almost the same as that for the perfect ones. The calculated normalized spectrum and the experimental data for $\Delta\psi=1.759°$ and $\Delta\phi=0°$ are shown in Fig. 12, where the HF form factor is used in the calculation. The difference between the theoretical curve and the experimental data in the vicinity of the peak is slightly larger than that for the perfect silicon crystal. The difference between perfect and imperfect silicon crystals is found to be so small that our method is applicable to such a metal crystal that has its dislocation density of the order of magnitude similar to that of the present imperfect silicon crystal.

D. Possible improvement of experimental methods

As discussed in the earlier section, the present set-up and the theory are enough to determine the atomic form factor of silicon to the level of few percents. Though this accuracy is insufficient for silicon but is readily useful for obtaining information of form factors for certain crystals, such as Ni, Al and Zn, to which we cannot apply the *Pendellösung* method.

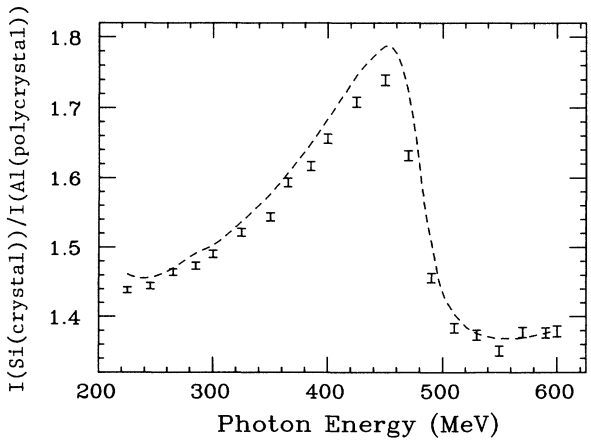

FIG. 12. Normalized spectrum of imperfect Si crystal under almost the same condition for the perfect one as shown in Fig. 9.

The shortcoming of the present method is in the theoretical treatment which includes uncertainties of the order of α, the fine-structure constant, implying that the comparison between calculated and experimental results is valid only to a few percent level. We need the terms of the second order in α to discuss the results within an accuracy of 0.5%.

In this experimental set-up, the beam cannot have the shape optimized for our experiment. As a result, the crystal must be thin and large in its perfect area. These constraints confine the kind of crystals to be measured in the present set-up, but are not essential since use of more dedicated beam line can easily get rid of them.

VI. CONCLUSION

We have developed a new method to determine the atomic form factor by means of precise measurement of the coherent bremsstrahlung. Counting the recoil electrons of Übeall effect, we obtained photon-energy spectra easily in a short time with strict reproducibility. The form factor was determined by modifying the HF form factor around the lowest reflection point so as to reproduce the experimental spectra. The change of experimental result due to the radiation damage of the target crystal was not observed. The shape of the coherent spectra from the silicon crystal has been reproduced excellently by a theoretical calculation which uses the HF form factor modified by about 3.3% at 111 reflection. This change qualitatively supports experimental results from *Pendellösung* method by Saka and Kato,[10] although quantitatively the deviation from the HF form factor in our case disagreed with that in the latter case by about 1.3%, which is just of the order of ambiguity in the theoretical calculations to be compared with our experimental results. From these observations, if properly improved, the present method is very promising for high-precision determination of atomic form factor.

For the imperfect silicon crystal, we obtained a spectrum very similar to that for the perfect one. The difference is so small that we can apply the method to such a crystal that the dislocation density is of the order of 10^4 cm^{-2} We conclude that our procedure has a good reliability and will be valid for many crystals. In addition, our final emphasis is that the present method enables us to obtain information complementary to that obtained from ordinary x-ray measurements.

ACKNOWLEDGMENTS

The authors would like to express their sincere appreciation to Professor H. Motegi and Mr. M. Kimura of Shin-etsu Handoutai Co. Ltd., who kindly provided us with perfect and heavily dislocated silicon crystals. The operating crew of the INS synchrotron are gratefully acknowledged. The data analysis was mainly performed by using the computers of the Data Analysis Laboratory for High Energy Physics, Hiroshima University.

[1]D. C. Creagh and J. H. Hubbell, Acta Crystallogr. **A43**, 102 (1987).
[2]D. T. Cromer and J. B. Mann, Acta Crystallogr. **A24**, 321 (1968).
[3]J. A. Ibers, in *International Tables for X-Ray Crystallography*, edited by MacGillavry, Rieck, and Lonsdale (Kynoch, Birmingham, England, 1962), Vol. III, pp. 201–212.
[4]J. H. Hubbel *et al.*, J. Phys. Chem. Ref. Data **4**, 471 (1975).
[5]D. Watanabe, R. Uyeda, and M. Kogiso, Acta Crystallogr. **A24**, 249 (1968).
[6]T. Kifune *et al.*, J. Phys. Soc. Jpn. **21**, 1905 (1966).
[7]G. Bologna, G. Lutz, H. D. Shultz, U. Timm, and W. Zimmermann, Nuovo Cimento **A42**, 844 (1966).
[8]R. Voss, G. Lehmpfuhl, and P. J. Smith, Z. Naturforsch. **35a**, 973 (1980).
[9]I. Endo *et al.*, Phys. Rev. Lett. **60**, 2292 (1988).
[10]T. Saka and N. Kato, Acta. Crystallogr. **A42**, 469 (1986).
[11]M. Hart, Z. Phys. **189**, 269 (1966).
[12]T. Takama and S. Sato, Aust. J. Phys. **41**, 433 (1988).
[13]H. Bethe and W. Heitler, Proc. R. Soc. London **A146**, 83 (1934).
[14]U. Timm, Fortsch. Phys. **17**, 765 (1969).
[15]K. Yoshida *et al.*, IEEE Trans. Nucl. Sci. **32**, 2688 (1985).
[16]I. Endo *et al.*, Phys. Lett. A **146**, 150 (1990).